Peculiarities of aluminum particle combustion in steam

Fabien Halter, Valentin Glasziou, Marco Di Lorenzo, Stany Gallier, Christian Chauveau

Peculiarities of aluminum particle combustion in steam

Fabien Halter[a,b], Valentin Glasziou[a,c], Marco Di Lorenzo[a], Stany Gallier[d], Christian Chauveau[a*]

[a]*CNRS – ICARE, 45071 Orléans, France*
[b]*Université d'Orléans, 45100 Orléans, France*
[c]*CEA, DAM, CEA-Gramat, 46500 Gramat, France*
[d]*ArianeGroup, 91710 Vert le Petit, France*

Abstract

This work experimentally addresses aluminum combustion in steam, pure or mixed with diluents, for aluminum particles in size range 40~80 µm, using an electrodynamic levitator. High-speed videos unveil an unreported and complex mechanism in steam, not observed in other oxidizers. The detached flame is quite faint and very close to the surface. Alumina smoke around the droplet rapidly condenses and coalesces into a large, single orbiting alumina satellite. It eventually collides the main aluminum droplet while generating secondary alumina droplets. A unique feature is the presence of several distinct oxide lobes on the droplet, which merge only at the end of burning and encapsulate the remaining aluminum, possibly promoting an incomplete combustion. The measured burning times in pure water vapor are longer than expected and the efficiency of steam is found to be 30 % that of oxygen, lower than the usually accepted value of 60 %. A general correlation on burning time, including the major oxidizers, is proposed. Direct numerical simulations are conducted and are in line with experiments, in terms of burning rate or flame stand off ratio. Combustion in steam seems mostly supported by surface reactions, giving a faint flame with low gas temperatures and high hydrogen content. It is speculated that those two specific features could help explain the peculiarity of steam.

Keywords: Aluminum combustion; Steam; Burning time; Oxidizer efficiency

---

*Corresponding author.

1. Introduction

Aluminum is usually added to solid rocket propellants or high explosives to increase performance. Aluminum particles burn within the gas released by the decomposition of those energetic materials. The predominant components of this region are CO_2, H_2O, and HCl. The precise determination of the dependence of oxidizer concentration on aluminum combustion is vital to our predictive ability in this area. The oxidizers considered to be efficient in aluminum combustion are O_2, CO_2, and H_2O.

Previous authors have suggested many ways in which oxidizer concentrations should be included in a global correlation predicting the burn time of an aluminum particle. Pokhil et al. [1] suggested combining the respective oxidizer mole fractions into one term. However, weighting all oxidizers the same was demonstrated to be inappropriate as each oxidizer has been seen experimentally to have a different effect on the burn rate [2]. Brooks and Beckstead [3] suggested a correlation in which the oxidizers are weighted to account for a global effect and was then followed by Widener and Beckstead [4] who proposed in addition to raise the "effective oxidizer concentration" in the correlation to a power to account for the non-linear dependence of burn time on effective oxidizer concentration.

Oxygen has been demonstrated to be the strongest oxidizer and consequently, burning an aluminum particle in a pure O_2 environment leads to the shortest combustion times. The oxidizer efficiency of O_2 is historically considered equal to unity and the respective oxidizing efficiency of other oxidizers are estimated relative to this reference. The relative strength of CO_2 and H_2O, which are much more available than O_2 in a SRM, is less clear. Widener and Beckstead [4] indicate that the physical reasons for the differences in each oxidizer's effect on burn time are first, the differences in heats of reaction, and to a lesser extent the differences in diffusivities. For each O_2 molecule that diffuses to the particle surface, two oxygen atoms will be available to react with aluminum, whereas only one oxygen atom will be available to react for both CO_2 (assuming the formation of CO) and H_2O. Therefore, diffusion will have to occur twice faster in CO_2 and H_2O to release the same amount of oxygen. Note that water vapor has a relatively high diffusivity in relation to the other oxidizers. Brooks and Beckstead [3] showed that for a given oxidizer concentration the burn rate is highest for O_2, followed by H_2O, and finally CO_2. Lynch et al. [5] proposed a correlation based on measurements in H_2O/Argon. Their correlation assigns a relative oxidizer efficiency of H_2O and CO_2 to O_2 with water being about half as effective and CO_2 about a fifth as effective. Bazyn et al. [6] did not end up with the same ranking: oxygen was found the most reactive followed by CO_2 and finally H_2O. As it can be seen, the relative oxidizing strength of water vapor has not been clearly established, mainly because of the scarce amount of data available. Moreover, very few experimental measurements at the scale of a particle are available in the literature, in particular for atmospheres with 100% H_2O. To our knowledge, only two experimental studies provided information of Al particles burning in steam. In 1999, Bucher et al. [7] observed that a freely falling Al particle burning in steam exhibit a reduced reactivity in the gas phase with a non-symmetrical flame structure. Gill et al. [8] also observed a decrease in luminous intensity of particles burning in water vapor atmospheres compared to CO_2 and O_2 environments. However, these two studies do not directly provide information on burning time. The rest of the research for oxidizers containing water vapor containing has been undergone in the post flame gases of a gas burner or propellant mixture, where water vapor was always mixed with other gases.

The current study affords new insights of aluminum particles combustion in pure water vapor environment and details the processes at play on the droplet scale. This type of Al/H_2O combustion is critical in the design of propulsion systems and is also of great interest in the context of "green" propulsion, under water or on Mars [9]. To our knowledge, this study is the first one to gain detailed information (phenomenology and burning times) on aluminum combustion in pure water vapor.

2. Experimental device and associated diagnostics

2.1 Experimental setup

This device has already been described in detail and we invite the reader to consult reference [10]. The experimental device is mainly composed of a high-pressure combustion chamber in which an electrostatic levitation system is inserted, and of a laser ignition system. The particles, initially charged with triboelectric effect, are introduced in the electric field in the center of the levitator. Then, a single particle is isolated in the center of the chamber by modulating the different voltages of the levitator. The position of the particle is crucial, because it must correspond exactly to the position of the focusing point of the ignition laser. The laser used is a CO_2 laser, with a power of 50 W, with a wavelength of 10.6 µm. The particle stabilized in levitation is heated uniformly on both sides thanks to the laser beam initially divided in two. The duration of the laser emission is controlled by an external trigger set by the light emission captured by the photomultipliers (PM) (described in the following paragraph). The high-pressure chamber (up to 12 MPa by design) allows combustion experiments to be conducted in a controlled gaseous atmosphere, and with a wide variety of gas composition. Historically, this chamber was not designed to

operate at high temperatures. In order to be able to work with gaseous atmospheres containing water vapor, a number of modifications to the experimental setup are made and described in the following.

2.2 Improvements to the experimental setup

In order to contain a water vapor environment, the high-pressure chamber must be heated to a temperature above that corresponding to the saturation vapor pressure curve. The heating of the high-pressure chamber is ensured by a heating corset by Joule effect and an insulating envelope limiting the thermal losses towards the outside. The installed power is 1450 W, allowing considering a maximum temperature of 500 K. In addition to this main element, all the pipes are also heated by spiral heating wires around the pipes, and then thermally insulated.

An additional system has been installed on the experimental device, it concerns the steam generation device. This device consists of a brass block with a small volume cavity (25 cm^3), and heated by two heating cartridges of 150 W each. This tank is connected to the high-pressure chamber by a pipe also heated, to avoid any possibility of condensation. Valves located upstream and downstream, allow the isolation of the tank of the whole, and thus allow the preparation of a volume of steam, ready to be injected.

In order to achieve precise and homogeneous temperature values, a central temperature control system with PID controllers has been implemented. A system of three PID controllers and three thermocouples allows the temperature of the chamber, the pipes and the tank to be regulated independently. In addition, a fourth thermocouple was installed to measure the gas temperature inside the chamber. This system has been calibrated and tested, and has demonstrated its ability to control the temperature accurately and stably over a wide range of temperatures.

Different gas compositions could be examined, with various contents of H_2O vapor. The concentration of each component is determined by the distribution of the respective partial pressures of each gas. However, a specific procedure has been established to introduce the steam in the best conditions. First of all, the whole apparatus, the chamber and all the pipes are evacuated. Then the chamber is filled with the chosen diluent gas (CO_2 or Ar) at the partial pressure of the desired mixture. A long waiting time (1-2 h) is then necessary, so that the temperature stabilization of the whole apparatus is reached. Then the necessary amount of steam is added to reach the desired final pressure. Then a period of temperature stabilization is necessary before starting the first particle combustion experiments.

2.3 Diagnostics & data processing

The measurements are mainly based on optical diagnostics. First, PM HAMAMATSU R2752 tubes equipped with optical filters are used to transform the collected radiative emissions into voltage signals and to provide information on the evolution of the light trace of the particle during the combustion process. After amplification, a USB-1808X acquisition card (Measurement Computing) is used to digitize the signal on 18 bits with a resolution of 75 µV and a frequency of 100 kHz. The temporal follow-up of the evolution of the burning particle is ensured by the use of an imaging device coupling a fast camera PHANTOM combined with a long-distance microscope QUESTAR QM100 focused on the particle in reaction. Two different cameras were used during this study allowing to obtain high acquisition speeds. The first one is a PHANTOM V2512 from 25000 fps at maximum resolution (1280x800 px) to 75600 fps at minimum resolution used during this study (512x512 px). The second camera used is the PHANTOM TMX 7510, allowing 76000 fps at maximum resolution (1280x800 px) to 450000 fps at the resolution used in this study (512x128 px). The magnification obtained with the long-distance microscope is 2 µm/px for the V2512 and 1.32 µm/px for the TMX 7510. The two optical diagnostics are synchronized temporally by the initial trigger of the experiment, and thus allow a direct comparison between the images and the light emission signal collected by the PM.

The images obtained by the fast camera allow not only a phenomenological description of the combustion process, but also, after the application of a numerical treatment, the extraction of quantitative information such as for example the diameter of the initial aluminum particle after melting, the temporal evolution of this diameter, the migration speed of the alumina particles towards the drop, etc.

3. Specificity of the combustion of an Al particle in steam

3.1 Phenomenology of specific alumina production and comparison with other oxidants

An aluminum particle is isolated and stabilized in the center of the levitator. The particles studied here have a size between 30 and 80 µm. The surrounding gas is mainly composed of water vapor with parametric variations in the percentage of the diluent used. We examined the steam coupled with CO_2 (25%, 50% and 75%), as well as steam with argon (50%). The phenomenology encountered is globally the same and we will describe here in more detail the combustion of an Al particle in an environment of 100% steam (Fig.1). The pressure and temperature conditions are respectively 1 atm and 410 K.

The initial morphology of the particle is not necessarily spherical. Thus, when subjected to CO_2

laser heating, the first observable step will be the melting and subsequent spherization of the particle. This change of state of aluminum oxide is accompanied by a migration and convergence of the different islands to form a floating lobe on the surface of the aluminum drop exposed to the oxidizing environment (Fig 1, image 1). A diffusion flame is instantly created around this drop. The particularity observed here is that the location of the flame is closer to the surface of the drop than in the other gaseous environments previously explored. This will be detailed later.

Moreover, the observation usually made in other gaseous environments is that alumina produced in the diffusion flame condenses in nanometric form and presents a uniformly distributed and homogeneous light front. The phenomena observed in the context of steam are completely different. The products of combustion do not condense uniformly but on localized sites, which concentrate almost instantaneously and gather in agglomerates of increasing size around the aluminum drop (image 2). Rapidly the successive coalescence of these agglomerates leads to the growth of a single globule, orbiting around the drop, but diametrically opposed to the initial lobe (image 13) (due to reduced alumina production in the vicinity of the lobe). This phenomenon seems to be also observed in Fig. 2 of Bucher et al. [7]. Those processes of homogeneous nucleation and condensation growth of particles have been modeled by Storozhev and Yermakov [11]. Then, this globule of alumina ends up colliding the surface of the aluminum, the forces of wettability then lead to the formation of a secondary lobe (image 16). We can then observe two concomitant phenomena that we now describe separately in the following paragraphs: splashing and multi-lobes.

3.1.1 Crown Splashing.

When the alumina globule contacts the aluminum surface, it partially covers an area of the drop in the form of an additional lobe. But this transition is very often accompanied by the generation of secondary droplets of alumina distributed in a crown (image 5), very similar to those observed during the splashing phenomenon of a drop on a flat surface, and very widely described in the literature [12, 13]. The droplets released during splashing are caught in a string of droplets orbiting the drop and then describing the same process of migration, coalescence and formation of a globule (image 7).

3.1.2 Multi-lobed and Lobes Overlap

The other phenomenon observed, which is quite unusual, is the fact that the secondary alumina lobes do not merge instantly with the lobe already present. We are left with a drop of aluminum with several lobes of alumina on its surface, thus reducing its surface exposed to the oxidant. We could observe on many occasions the presence of 3 or 4 lobes simultaneously (image 9). Then they progressively merge, with stable positions at the two opposite poles of the aluminum drop (image 18). Some possible explanations for this multi-lobed configuration are proposed in the forthcoming Discussion Sec.5.

3.1.3 Incomplete Combustion

This so-called "bipolar" configuration is established in a quasi-steady manner, and we then observe a relatively stable combustion, with the aluminum zone exposed to the oxidizer in the form of a central ring, which is reducing as the lobes grow. These lobes follow more and more the shape of the drop, and tend towards a progressive encapsulation. Finally, when this interstitial zone becomes very small, the lobes are tilted (image 20), and they merge and end up covering almost completely the aluminum drop (image 21). Eventually, alumina covers the entire drop, and presumably leads to a complete extinction of the particle. A late increase of the residue luminous intensity is always observed prior to full extinction. It is attributed to the exothermal alumina phase transition from liquid to solid. This peculiar instant has been selected to identify the end of the combustion.

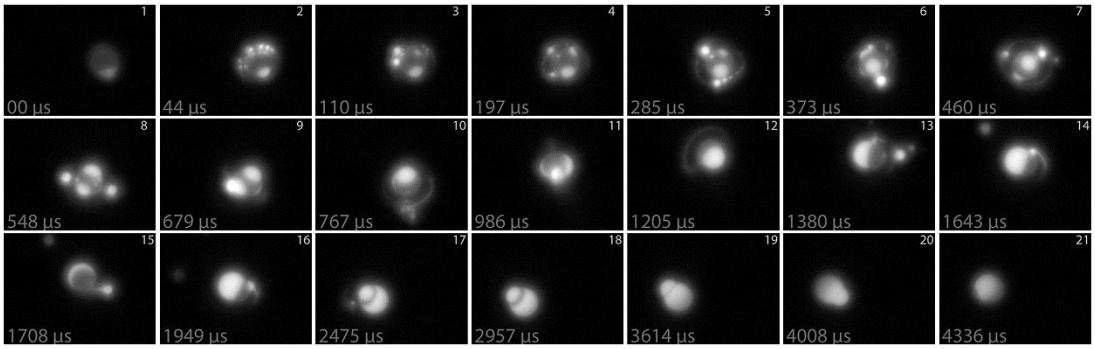

Fig 1: Images extracted from a combustion sequence of an Al particle in a 100% steam atmosphere.
(d_0 = 52 µm, sequence captured at 230 000 fps)

3.2 Vaporization rate and Stand off ratio determination

The combustion time t_b is defined between the extinction of the CO_2 laser and the solidification of the oxide residue (see previous remark). It is estimated based on photomultiplier signals (PM), i.e. direct light emission. The moment of solidification being clearly detectable on all the sequences, this criterion seems more robust than those proposed by Olsen and Beckstead (constant height, percent area, percent height) [14]. Figure 2 compiles experimental burning times for different oxidizers at 1 atm. Experiments in the presence of water vapor were performed at 410 K whereas the others (i.e. O_2 and CO_2) at 300 K. According to Beckstead's correlation [15], the initial temperature effect is low (power exponent of 0.2). Correcting our experimental results to account for the temperature difference would decrease the combustion time by around 6%. This was not done in Figure 2 to keep original experimental values.

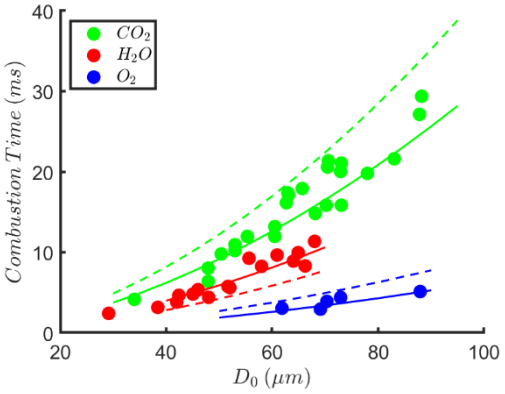

Fig. 2. Measured burning time with particle diameter for different pure oxidizers (symbols). Dashed Lines: Beckstead's correlation [15]. Solid Lines: updated correlation from ICARE [10].

In the figure are also presented Beckstead's correlations [15] in dashed lines for the three oxidizers accounting for the different initial temperatures. Slight differences are observed between this correlation and our experimental results, namely an overestimation of the combustion time for both O_2 and CO_2. On the contrary, combustion times in steam are underestimated meaning that H_2O reactivity is overestimated using Beckstead's correlation. Note that the latter correlation, based on 400 datum points, does not include data obtained for pure steam conditions. The maximal water content considered was 89% with the rest being oxygen (hot burnt gases of H_2/O_2 mixtures). Moreover, the number of measurements including steam is low, which might explain this reduced accuracy. Additional experiments have been performed for varying CO_2/H_2O environments (50/50 – 75/25). Combustion times obtained for these CO_2/H_2O mixtures (not presented there) are located between those of pure gases. However, the experimental variability does not make it possible to provide a clear evolution.

We have incorporated into our recently proposed correlation [10] (based on more than 300 experiments for O_2, CO_2, CO and/or N_2 environments) water vapor results (pure and blended environments) which corresponds to around 30 additional data points, half of which is pure steam. The modified correlation from [10] (solid lines called ICARE in Figure 2) fits our current results well. The combustion time (t_b) is expressed as (with units: atm-K-ms-µm):

$$t_b = \frac{0.00626\ {D_0}^{1.75}}{X_{eff}\ P^{0.07}\ T^{0.2}} \qquad (1)$$

where D_0 is the initial droplet diameter, and

$$X_{eff} = X_{O_2} + 0.2\ X_{CO_2} + 0.3\ X_{H_2O} + 0.03\ X_{CO} - 0.01\ X_{N_2}$$

Keeping O_2 oxidizing efficiency to unity, an efficiency of 0.3 is obtained for H_2O to be compared to 0.2 for CO_2. Beckstead [15] also found that CO_2 was only 22% as efficient as O_2 but proposed 60% for H_2O, which is clearly too efficient regarding our data.

A novelty of our setup is that image processing can also provide time-resolved evolution of particle diameter $D(t)$. Interestingly, this allows computing the evaporation rate $K = dD^2/dt$, which is the major input data for classical D^2 models.

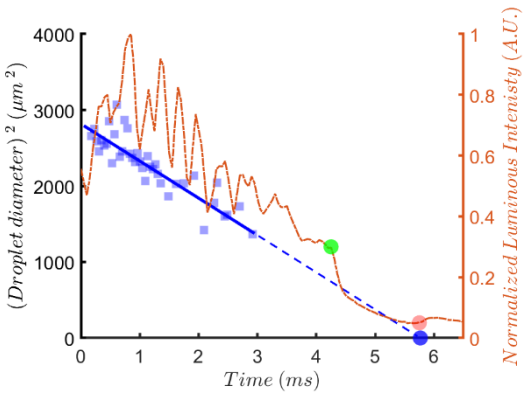

Fig. 3. D^2 (blue) and normalized light emission (red) evolutions for a 40 µm particle burning in steam (1 atm – 410 K).

Figure 3 illustrates the particle diameter regression (blue squares) of a 40 µm particle in steam (1 atm – 410 K). Initial time is phased with the laser switched

off. A linear fit (solid blue line) allows extrapolating the combustion time (blue dot). Red dashed line indicates the normalized direct light emission acquired by a PM at 488 nm. Light intensity is globally decreasing till extinction with strong oscillations resulting from the complexity of the phenomena at play as discussed in Part 3. The start of the residue solidification (last bump) is marked with a red dot. A combustion time similar to the one extrapolated (blue dot) is obtained. Note that this linear extrapolation assumes that a D^2 law holds, which may not be the case, strictly speaking. This is only a first approximation but it turns out to be consistent with information collected from light emission. Again, this plot does not imply that n is strictly equal to 2. All sequences of particles burning in steam exhibited similar results and afforded an evaporation rate of 0.5 ± 0.1 $mm^2/\mu s$.

Additional information such as the aluminum surface not covered by alumina may be estimated during the combustion process. We have observed that after 2 ms, the particle is covered by two opposite lobes (Fig. 1, image 17) and the 'free' surface available for aluminum vapor production becomes almost negligible. However, it is seen in Figure 3 that the light emission remains substantial and continues to present an important dynamics attesting of a reaction still in progress. The merging of two alumina lobes occurs after 4 ms (green dot in Fig. 3). One can assume that a slow cooling occurs after this point. Full understanding of these phenomena will need further investigations.

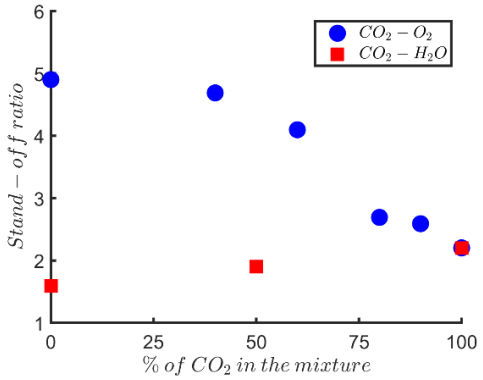

Fig. 4: Stand off ratio for different oxidizing environments (1 atm). Initial temperature of 410 K for mixtures with steam, 300 K otherwise.

Finally, the stand off ratio (flame diameter to the initial particle diameter) is evaluated in Fig. 4 as a function of the CO_2 content for both O_2/CO_2 and H_2O/CO_2 mixtures. Determining the flame diameter when burning in steam is delicate as the flame is very close to the aluminum droplet surface and not as bright as with other oxidizers. The flame diameter was defined as the most luminous zone in the flame zone, which is supposed to correspond to a maximum of alumina smoke fractions. Same definition was taken in part 4 to compare with simulation results. This observation was already done by other authors experimentally [8, 16] or numerically [4]. It is clear from Fig. 4 that the stand-off ratio decreases when adding water vapor to an H_2O/CO_2 mixture with a value around 1.6 for pure steam (whereas it is close to 5 for pure O_2).

4. Theory and simulations

This section provides some theoretical estimations, using standard D^2 theory, as well as preliminary simulations to help explain the previous observations.

Large aluminum droplets (typically, D>50 µm) are generally expected to burn through a diffusion flame. In this case, and under reasonable assumptions (spherical symmetry, quasi-steadiness, rapid chemistry...), the burning time t_b is found to scale as $t_b = D^2/K$ with the evaporation constant K given as [17]:

$$K=8\,\rho_g\mathscr{D}/\rho_l\,\ln(1+B) \qquad (2)$$

where ρ_g and $\mathscr{D}$ are the gas density and fuel diffusivity on the droplet surface and ρ_l is the liquid aluminum density. We take $\rho_g\mathscr{D}$=1.6.10^{-4} m^2/s and ρ_l=1500 kg/m^3. The Spalding number B is defined as $B=(Q\ sY_{\infty,ox}+c_p(T_s-T_\infty))/L_v$ with c_p the droplet heat capacity (here taken to 1200 J/(kg.K), T_s its surface temperature (~2500 K) ; T_∞=300 K and $Y_{\infty,ox}$=1 are the upstream temperature and oxidizer fraction. Q and s are the heat of reaction and fuel/oxidizer stoichiometric ratio. For O_2, CO_2, and H_2O, Q is respectively 39, 24, and 25 MJ/kg while s is 1.12, 0.41 and 1. The latent heat of vaporization is L_v=10.9 MJ/kg.

Table 1
Experimental and predicted K and stand off ratio in pure gases (p=1 atm).

Gas	K ($mm^2/\mu s$)			D_f/D_0	
	Exp.	Theo.	Sim.	Exp.	Sim.
O_2	2.1±0.7	1.33	1.68	4.9	5.0
CO_2	0.3±0.05	0.43	0.35	2.0	2.1
H_2O	0.5±0.1	0.95	0.60	1.6	1.4

The obtained results on K are compiled in Tab. 1 (column label "*Theo.*"), with measurements ("*Exp.*") obtained in this study as well as in one of our previous works [10]. A good agreement is found for O_2 and CO_2, which is suggestive of a diffusion-controlled combustion complying with the D^2 framework. Conversely, combustion in steam is measured to be much slower than expected theoretically (0.5 vs. 0.95 $mm^2/\mu s$). This is a deviation from classical diffusion-limited combustion and suggests some specific features of combustion in H_2O. Note that Eq. (2) should not hold strictly because the aluminum particle is not

spherical due to the existence of the oxide lobe. Theoretical estimations of *K* must therefore be viewed as first crude approximations.

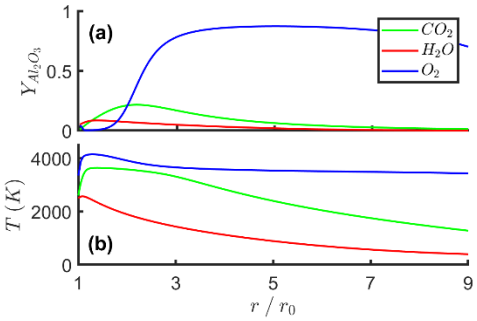

Fig. 5. Alumina mass fraction (a) and temperature (b) profiles as a function of the normalized distance to the droplet surface.

Beyond this preliminary simple analytical step, we have also considered direct numerical simulations of a single, spherical, burning aluminum droplet by solving the two-dimensional axisymmetric reactive Navier-Stokes equations around the droplet. Note that the simulations conducted here are not intended to be a detailed, dedicated study but are rather preliminary simulations to provide a first level of information for discussion. Numerical details are skipped for brevity and details have been already given in [18]. The present simulations closely follow the ones described in this reference, including grid, numerical parameters, transport coefficients or kinetics.

A D=220 µm droplet is considered at p=1 atm in various pure oxidizers: O_2, CO_2 and H_2O in order to highlight the main differences. The exact mechanism can be found in [18] and is taken as is. For the gas phase, it includes 51 reactions and 22 species. This droplet configuration was chosen for convenience as a first step since it has been described in detail in [18]: future works need however to check whether size can alter our conclusions since droplets studied experimentally are slightly smaller (40~70µm).

Combustion in O_2 and CO_2 is self-sustained, which is not the case for H_2O. Combustion in steam could only be maintained with the help of surface reactions. The surface mechanism is a subset of Ref. [18] for water: it includes 35 reactions and 13 species. Simulations suggest that combustion in H_2O is controlled by kinetically limited surface reactions. This is a first distinctive difference of steam, which supports the idea that aluminum combustion primarily follows a heterogeneous route, as surmised from the previous chapter. This heterogeneous nature is consistent with the faint flame noted in experiments.

Overall, the numerical results are presented in Tab. 1 in terms of evaporation constant *K* and stand off ratio (column "*Sim.*"). To be consistent with experiments, the flame is here defined as the maximum of alumina (Al_2O_3) smoke fraction.

There is a good match between simulations and measurements of *K* as well as the flame position. This suggests that simulations might include the major physics, and in particular the importance of surface reactions for water. It is interesting to note that the burning rate (hence, constant *K*) in steam is relatively lower than theoretically expected, but in line with experiments.

Temperature and alumina smoke fraction profiles are given in Fig. 5. Unlike O_2 and CO_2, combustion in H_2O is virtually flameless with a maximum gas temperature slightly below 2600 K, unlike about 3500 K and 4150 K for CO_2 and O_2, respectively. In steam, combustion seems sustained by surface reactions without any significant flame. Therefore the maximum temperature is on, or close to, particle surface and it remains low due to the absence of significant gas reactions.

In steam, the smoke concentration profile is also quite low, pretty flat, and very close to the surface in qualitative agreement with experiments. The droplet temperature is found to be 2660 K, 2520, and 2450 K for O_2, CO_2 and H_2O, respectively. Simulations in steam [18] predict small oxide residue (hence, small lobe); this is clearly not the case experimentally, which suggests that the physics is complex and that kinetic model in [18] might be enriched.

This theoretical and numerical work clearly needs to be deepened; this is part of our future works. This must only be viewed as a preliminary step, in order to provide a first level of information to support the forthcoming discussions.

5. Discussions

We here provide discussions on the noted specific features of aluminum combustion in water vapor.

A first peculiarity is the existence of multi-lobed droplets. Experiments attest large alumina satellites located between 1 and 2 radii from the droplet, which, from the simulations, corresponds to gas temperature in the range 1500~2000K. Their diameter is about 15~25 µm, which gives a characteristic time scale for thermal inertia of 200~600 µs. From the experiments, a typical time scale for moving back to the main droplet is 10~20 µs, i.e. much smaller, meaning that alumina satellites may keep their initial temperature for some time. This difference in temperature probably involves gradients in surface tensions, which could promote Marangoni stresses and hinder lobe merging.

It is, however, not well known what makes such orbiting alumina satellites move back to the burning droplet, against the Stefan flow induced by the aluminum evaporation (outward velocity on the aluminum particle surface due to the prevailing reaction $Al_{(liq)} \rightarrow Al_{(gas)}$). Simulations confirm that the

Stefan flow velocity is slightly smaller in the water case (about 4 m/s, against 6 m/s for CO_2 and 30 m/s for O_2). Thermophoresis can usually be significant [19] but owing to the absence of strong temperature gradients in H_2O, it is weak and would anyway move alumina outwards here. A specificity of combustion in steam, however, is the massive production of light species, notably H_2, which is predicted to reach a molar fraction as high as 0.25 on droplet surface. This opens the possibility for a diffusiophoresis where small alumina particles are convected along concentration gradients. Because H_2 concentration is higher close to the aluminum surface, alumina particles are expected to move towards the droplet. We have considered an expression by Whitmore [20] for the diffusiophoretic velocity in multicomponent mixtures and applied it to our simulation results. A maximum value of about 1 m/s was found in the H_2O case with the velocity pointing towards the droplet, as expected from experiments. This is still lower than the Stefan velocity but this value is sufficiently significant to foster further inspection and consider diffusiophoresis as a possible mechanism explaining alumina particle motion in water vapor.

Another intriguing feature of combustion in water vapor is that the aluminum droplet can be completely encapsulated by the oxide lobes, which was not noticed in other gases. For an immiscible binary droplet, alumina can engulf aluminum if $S=\sigma_{Al2O3} + \sigma_{Al/Al2O3} - \sigma_{Al} < 0$ [21]. Surface tensions σ for liquid aluminum, liquid alumina, and aluminum/alumina are known functions of the temperature [22]. For temperatures of interest (~2500 K), S is found to be positive and about +0.2 N/m, excluding the possibility of encapsulation. However, if σ_{Al} is slightly higher, S can turn negative indicating the possibility of encapsulation by alumina. We find that a 25 % increase is necessary to have a negative S. A possible explanation could be related to different aluminum/alumina temperatures (as discussed previously) or change in the composition of the molten aluminum, for instance due to atomic hydrogen H diffusing into the aluminum lattice [18].

6. Conclusions

This work seems the first study to garner detailed information (high-speed videos and burning times) on aluminum combustion in pure steam. Experiments suggest very peculiar features, not reported in other oxidizers, such as smoke coalescence into an oxide satellite, multilobed aluminum droplet, or aluminum encapsulation by oxide. Burning times are relatively long, typical of that of carbon dioxide, and the oxidizer efficiency is found to be 0.3 that of pure oxygen (lower than the 0.6 from the usual Widener-Beckstead correlation). Simulations suggest a heterogeneous route with no or weak diffusion flame, low gas temperature and high hydrogen content. It is speculated that those specificities are likely to explain some of the observed mechanisms. Those new results suggest that aluminum combustion in steam is more complex than expected and this first study should stimulate further research. The effect of ambient pressure and temperature as well as other mixtures is worth considering as a future work. Measurements of temperature or species around the droplet could help confirm simulations and would be pivotal in gaining further understanding.

Acknowledgements

S.G. thanks the French Defense Procurement Agency DGA (*Direction Générale de l'Armement*) for funding. V.G. acknowledges the CEA for its financial support. We are also thankful to the Region Centre Val de Loire and the French Government Program "Investissements d'avenir" through the LABEX CAPRYSSES ANR-11-LABX-0006-01.

Supplementary material

The movie of the combustion of an aluminum particle burning in a steam atmosphere corresponding to the sequence of Fig. 1 is available as online supplementary material.

References

[1] P.F. Pokhil, A.F. Belyaev, Y.V. Frolov, V.S. Logachev, A.I. Korotkov, Combustion of powdered metals in active media, *URSS FTD-MT-24-551-73* (1973) 1-395.

[2] P.L. Micheli, W.G. Schmidt, Behavior of aluminum in solid rocket motors, *Aerojet Solid Propulsion Co* AFRPL-TR-76-58 (1977).

[3] K.P. Brooks, M.W. Beckstead, Dynamics of aluminum combustion, *J. Propul. Power* 11 (1995) 769-780.

[4] J.F. Widener, M.W. Beckstead, Aluminum combustion modeling in solid propellant combustion products, *AIAA Journal* 3824 (1998).

[5] P. Lynch, N. Glumac, H. Krier, Combustion of 5-micron Aluminum Particles in High Temperature, High Pressure, Water-Vapor Environments, in: 43rd AIAA/ASME/SAE/ASEE Joint Propulsion Conference & Exhibit, American Institute of Aeronautics and Astronautics, 2007.

[6] T. Bazyn, N. Glumac, H. Krier, in: 41st AIAA/ASME/SAE/ASEE Joint Propulsion Conference and Exhibit, 2005.

[7] P. Bucher, R.A. Yetter, F.L. Dryer, E.P. Vicenzi, T.P. Parr, D.M. Hanson-Parr, Condensed-phase species distributions about Al particles reacting in various oxidizers, *Combust. Flame* 117 (1999) 351-361.

[8] R.J. Gill, C. Badiola, E.L. Dreizin, Combustion times and emission profiles of micron-sized aluminum particles burning in different environments, *Combust. Flame* 157 (2010) 2015-2023.

[9] T.F. Miller, J.D. Herr, Green rocket propulsion by reaction of Al and Mg powders and water, *AIAA 2004-4037* (2004).

[10] A. Braconnier, S. Gallier, F. Halter, C. Chauveau, Aluminum combustion in CO2-CO-N2 mixtures, *Proc. Combust. Inst.* 38 (2021) 4355-4363.
[11] V.B. Storozhev, A.N. Yermakov, On the interplay of chemical and physical processes during the combustion of aluminum in water vapor, *Russ. J. Phys. Chem. B* 8 (2014) 672-679.
[12] C. Josserand, P. Ray, S. Zaleski, Droplet impact on a thin liquid film: anatomy of the splash, *J. Fluid Mech.* 802 (2016) 775-805.
[13] H. Yuan, J. Li, X. He, L. Chen, Z. Wang, J. Tan, Study of droplet splashing on a liquid film with a tunable surface tension pseudopotential lattice Boltzmann method, *AIP Advances* 10 (2020) 025209.
[14] S.E. Olsen, M.W. Beckstead, Burn time measurements of single aluminum particles in steam and CO2 mixtures, *J. Propul. Power* 12 (1996) 662-671.
[15] M.W. Beckstead, Correlating Aluminum Burning Times, *Combust. Explo. Shock Waves* 41 (2005) 533-546.
[16] P. Bucher, L. Ernst, F. Dryer, R. Yetter, T. Parr, D. Hanson-Parr, Detailed studies on the flame structure of aluminum particle combustion, *Solid propellant chemistry, combustion motor interior ballistics* 185 (2000) 689-722.
[17] K.K. Kuo, Principles of combustion, John Wiley & Sons, Inc., 2005, p. 732.
[18] J. Glorian, S. Gallier, L. Catoire, On the role of heterogeneous reactions in aluminum combustion, *Combust. Flame* 168 (2016) 378-392.
[19] S. Gallier, A. Braconnier, F. Godfroy, F. Halter, C. Chauveau, The role of thermophoresis on aluminum oxide lobe formation, *Combust. Flame* 228 (2021) 142-153.
[20] P.J. Whitmore, Thermo- and diffusiophoresis for small aerosol particles, *J. Aerosol Sci* 12 (1981) 1-9.
[21] J. Guzowski, P.M. Korczyk, S. Jakiela, P. Garstecki, The structure and stability of multiple micro-droplets, *Soft Matter* 8 (2012) 7269-7278.
[22] V.A. Babuk, V.A. Vasilyev, Model of Aluminum Agglomerate Evolution in Combustion Products of Solid Rocket Propellant, *J. Propul. Power* 18 (2002) 814-823.